Monday 18 May, late afternoon session

Ray Egerton Symposium: Elemental and ELNES 2D and 3D imaging
(Chairs: G. Botton, N. Browning)

16:30 **EELS imaging of biological structures in two and three dimensions (Invited)**
R.D. Leapman and M.A. Aronova
National Institutes of Health, Bethesda, MD, USA

17:00 **Atomic-scale chemical imaging of interdiffusion and defects in perovskite oxide heterostructures**
L. Fitting Kourkoutis[1], J.H. Song[2,3], Y. Hotta[2], T. Higuchi,[2] H.Y. Hwang[2,4], and D.A. Muller[1]
[1] Cornell University, Ithaca, NY. USA
[2] University of Tokyo, Chiba, Japan
[3] Chungnam National University, Daejeon, Korea
[4] Japan Science and Technology Agency, Kawaguchi, Japan

17:15 **EELS analysis of high-k dielectric systems**
A.J. Craven, M. MacKenzie, P. Longo and S. McFadzean
University of Glasgow, Glasgow, UK

17:30-17:45 *Break*

17:45 **High spatial-resolution analysis using STEM-EELS and ADF; Limit of incoherent imaging approximation (invited)**
K. Kimoto[1], K. Ishizuka[2], and Y. Matsui[1]
[1] National Institute for Materials Science, Tsukuba, Japan
[2] HREM Research Inc., Higashimatsuyama, Japan

18:15 **Basic questions involved in electron-induced sputtering**
R.F. Egerton[1,2], R. McLeod[1,2], F. Wang[2], and M. Malac[1,2]
[1] University of Alberta, Edmonton, Canada
[2] National Institute for Nanotechnology, Edmonton, Alberta

18:30 **Energy loss characterisation of nanostructures in 2D and 3D**
W. Guan, M. A. Mat Yajid, T. Gnanavel, Z. Saghi, Y. Peng, X. Xu, G. Möbus
University of Sheffield, Sheffield, UK

EELS imaging of biological structures in two and three dimensions

R.D. Leapman and M.A. Aronova

National Institute of Biomedical Imaging and Bioengineering, National Institutes of Health, Bethesda, Maryland 20892, USA

Elemental mapping by electron energy loss spectroscopy (EELS) provides useful quantitative information about biological structures in both normal and diseased states of cells and tissues. EELS imaging can determine the distributions of endogenous elements, e.g., phosphorus in nucleic acid-protein complexes that regulate transcription of genes in cell nuclei [1], calcium in membrane-bound compartments that regulate cell signaling processes [2], or iron in metalloprotein complexes that regulate cytoplasmic levels of trace metals such as iron [3]. EELS can also be applied to measure exogenous elements that are introduced into cells in nanomedicine applications, e.g., gadolinium attached to dendrimer nanoparticle-based contrast agents used in magnetic resonance imaging [4].

The choice of image acquisition mode, either fixed-beam energy-filtering transmission electron microscopy (EFTEM) or scanning transmission electron microscopy (STEM) depends on the type of application. For the analysis of smaller specimen regions, STEM-EELS enables precise modeling of the background underlying weak core-edge features, and offers high sensitivity with nearly single atom detection for certain elements like calcium and iron [5].

At the cellular level, structures of interest are often sparsely distributed, so that they occur infrequently within a given thin section. For such applications it is advantageous to employ EFTEM, which enables acquisition of compositional images from large areas containing around 10^6 pixels in times of order 100 s. To obtain accurate analyses from two-window EFTEM images, it is necessary to correct for shape changes in the spectral background caused by plural inelastic scattering [6]. EFTEM can be combined with electron tomography to provide quantitative three-dimensional elemental distributions within a sample volume, at a total dose that is comparable to that required to acquire a two-dimensional map [7].

Current studies emphasize development of correlative techniques based on fluorescence light microscopy, together with three-dimensional EFTEM and annular dark-field STEM. Such methods enable the study of biological systems across multiple length scales from the tissue to molecular levels [1, 8].

References

[1] Y. Ren et al., *J. Histochem. Cytochem.* 51 (2003) 605.
[2] A.P. Somlyo, *Cell Calcium* 6 (1985) 197.
[3] P. Zhang et al., *J. Struct. Biol.* 150 (2005) 144.
[4] H. Sarin et al., *J. Transl. Med.* 6 (2008) 80.
[5] R.D. Leapman, *J. Microsc.* 210 (2003) 5.
[6] M.A. Aronova et al., *Ultramicroscopy* 107 (2007) 232.
[7] M.A. Aronova et al., *J. Struct. Biol.* 160 (2008) 35.
[8] This research was supported by the Intramural Program of NIBIB, NIH

Atomic-scale chemical imaging of interdiffusion and defects in perovskite oxide heterostructures

L. Fitting Kourkoutis[1], J.H. Song[2,3], Y. Hotta[2], T. Higuchi,[2] H.Y. Hwang[2,4], and D.A. Muller[1]

[1] Applied and Engineering Physics, Cornell University, Ithaca, NY 14853, USA
[2] Advanced Materials Science, University of Tokyo, Kashiwa, Chiba 277-8561, Japan
[3] Department of Physics, Chungnam National University, Daejeon 305-764, Korea
[4] Japan Science and Technology Agency, Kawaguchi, 332-0012, Japan

In electron microscopy it is often difficult to distinguish between true intermixing and the apparent broadening of an interface due to the shape of the electron probe or its tails. However, with recent advances in aberration correction, full 2D spectroscopic images can now be recorded at atomic resolution in under a minute [1], and the additional chemical information can be used to directly detect chemical intermixing and its impact on the electronic structure of an interface.

Here, we present studies of the microscopic structure of oxide/oxide multilayers and heterostructures using spectroscopic imaging (SI), performed on a 5th order aberration corrected NION UltraSTEM 100. As an example, SI of an extended defect in a $La_{0.7}Sr_{0.3}MnO_3/SrTiO_3$ (LSMO/STO) multilayer is shown in Fig. 1. [2]

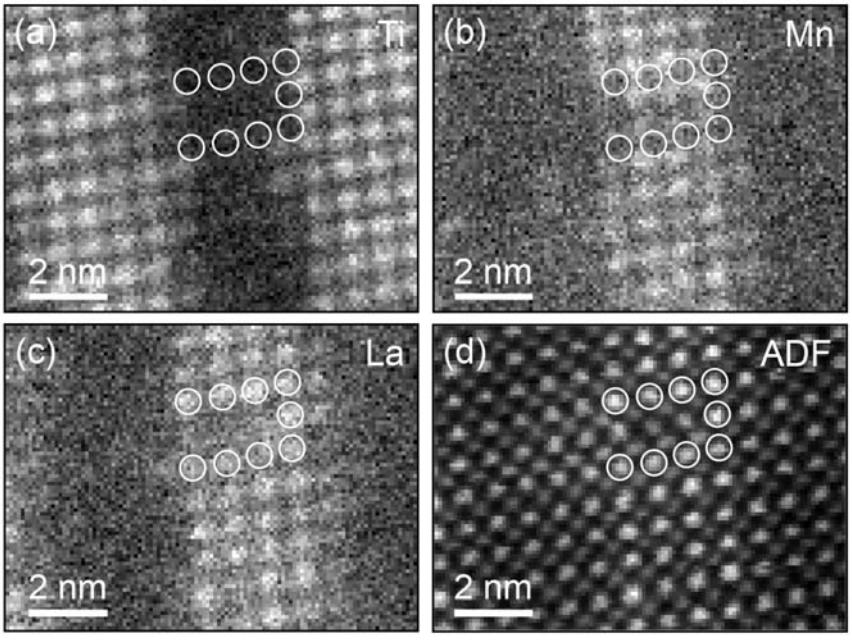

FIG. 1. Spectroscopic-imaging of an extended defect in a LSMO/STO multilayer. (a) Ti, (b) Mn, (c) La elemental maps extracted from an 109x80 pixel spectrum image and (d) the simultaneously recorded ADF image. The white open circles indicate the position of the La columns around the defect. The ADF image, which also tracks the position of the Sr atoms, shows clear atomic columns in the center of the defect, while the La concentration is low, suggesting that the defect was formed to accommodate for access Sr in the LSMO layer.

References

[1] D.A. Muller, L.F. Kourkoutis, M. Murfitt, J.H. Song, H.Y. Hwang, J. Silcox, N. Dellby, O.L. Krivanek, *Science* 319 (2008) 1073.

[2] Technical support by Niklas Dellby (Nion Co.) is gratefully acknowledged. LFK and DM supported by the ONR EMMA MURI and the Cornell Center for Materials Research, an NSF MRSEC. JHS, HYH supported by a Grant-in-Aid for Scientific Research on Priority Areas.

EELS analysis of high-k dielectric systems

A.J. Craven, M. MacKenzie, P. Longo and S. McFadzean

Dept. of Physics and Astronomy, University of Glasgow, Glasgow, G12 8QQ, UK

Metal (TiN, Ta_2N) inserted HfO_2-based high-k gate stacks on Si as well as Ga_2O_3/ $Ga_{2-x}Gd_xO_3$ gate stacks on III-V semiconductors (GaAs, InGaAs, AlInAs) are being investigated for current and future MOSFET applications. The wide range of atomic number and the interface roughness offer major challenges for high spatial resolution EELS spectrum imaging in these multilayer, nanometre-scale systems.

To deal with the range of edges present, it is essential to collect edges out to losses of ~2keV. Edges from some elements are difficult to extract but sometimes the ELNES on other edges can be used to give information on such elements. A further difficulty is the large change in scattering between a layer made up of mainly light elements and that from a layer made up of heavy elements. If the low loss spectrum is recorded at each pixel, it can be used to correct for this image contrast. It also allows the absolute numbers of atoms per unit area to be determined provided a suitable cross-section is available. In addition, it allows deconvolution of multiple scattering, which helps background subtraction and also gives the local thickness, provided a suitable inelastic mean free path is available. This allows the absolute numbers of atoms per volume to be determined.

An example is shown in Figure 1. Using the Glasgow dual EELS system [1], data were recorded from a Si/SiO_2/HfSiO/TiN/Si gate stack over the energy loss region -290 to +700eV in a line spectrum image with a pixel size of 0.5nm. The spectra were Fourier logarithmically deconvoluted and the intensities of the Si L-, N K- and Ti L-edges were obtained using power law backgrounds. For the O K-edge, power law backgrounds were fitted before the Ti L-edge and the Ti L-edge shape from unoxidised TiN was scaled and removed. The Hf content was determined from the O K-edge ELNES using HfO_2 and SiO_2 standards.

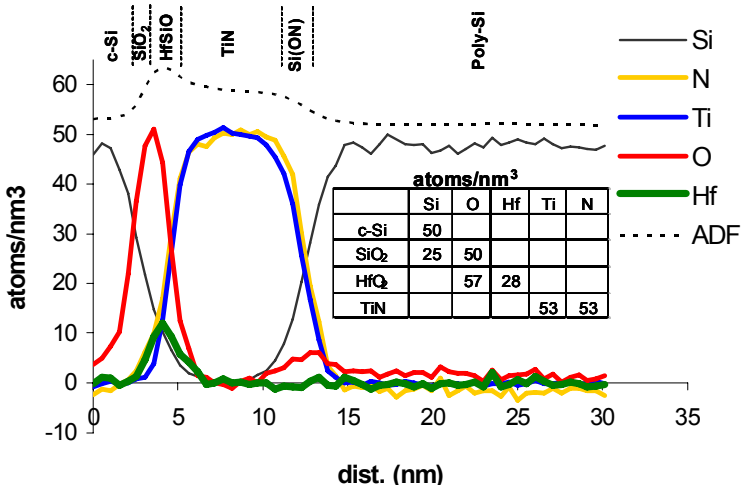

FIG. 1. Absolute numbers of atoms per nm^3 across a metal inserted high-k gate stack on silicon. The table gives the number of atoms per nm^3 in the bulk materials

[1] J. Scott et al *Ultramicroscopy* 108 (2008) 1586.

[2] This work was supported by EPSRC grants GR/S44280 and EP/F002610; the authors would like to thank Prof S de Gendt of IMEC for the material and Mr B Miller of Glasgow University for specimen preparation.

High spatial-resolution analysis using STEM-EELS and ADF; Limit of incoherent imaging approximation

K. Kimoto[1], K. Ishizuka[2], and Y. Matsui[1]

[1] National Institute for Materials Science,1-1 Namiki, Tsukuba, 305-0044, Japan.
[2] HREM Research Inc., 14-48 Matsukazedai, Higashimatsuyama, 355-0055, Japan.

Electron energy-loss spectroscopy (EELS) and annular dark-field (ADF) imaging in scanning transmission electron microscopy (STEM) are indispensable for material characterization with high spatial resolution. In both ADF and EELS, incoherent imaging model might be firstly assumed [1,2], in which an image is the convolution between the probe intensity profile and the object. Recent experimental results, however, suggest that the convolution model is not exactly valid for high-spatial-resolution domain. Here we show our experimental data obtained using STEM-EELS and ADF.

We followed EELS spectrum imaging scheme [3] for element-selective atomic-column imaging [4]. One of the important factors for realizing high spatial-resolution is the optimization of experimental condition to reduce delocalization in inelastic scattering. We demonstrated the effect of delocalization using the following materials. La atomic columns in $(La,Sr)_3Mn_2O_7$ are observed by using M_5-edge (832eV), but N_{45}-edge (99eV) intensity does not show the clear contrast [4]. Si atomic columns in β-Si_3N_4 cannot be visualized using the intensity of Si-L_{23} ELNES (103eV), but are resolved using the intensity at the EXELFS (>300eV) [5]. Delocalization in inelastic scattering means not only the large impact parameter, but inelastically scattered electrons are considered to be coherent, which is consistent to recent theoretical investigation [6]. Due to the coherent nature, contrast reversal in inelastic images is observed as well as bright-field (BF) images. Note that BF lattice fringe is preserved through low-loss scattering, and it was reported since the 70's [7,8].

ADF imaging are applied for crystal structure analysis of $(Tb,Ba)MnO_3$ [9], Eu-doped β-SiAlON [10], and $TmFeO_3$. Using high signal-to-noise ratio of STEM images, 10-pm atomic displacement can be detected [9]. The accuracy of the atomic position of ADF images depends on the incident probe propagation, which depends on the atomic arrangement around the atomic column of interest. In thick specimen, we have to reexamine the simple incoherent imaging approximation. Even in ADF imaging, specimen thickness should be minimized for intuitive interpretation.

[1] N. D. Browning et al., Nature 366 (1993) 143.
[2] S.J. Pennycook, D.E. Jesson, Ultramicrosc. 37 (1991) 14.
[3] C. Jeanguillaume, C. Colliex, Ultramicrosc. 28 (1989) 252.
[4] K. Kimoto, et al., Nature 450 (2007) 702.
[5] K. Kimoto, et al., Micron 39 (2008) 257.
[6] M. P. Oxley, et al., Phys. Rev. B 76 (2007) 064303.
[7] A. J. Craven, C. Colliex, Inst. Phys. Conf. Ser. 36 (1977) 271.
[8] K. Kimoto, Y. Matsui, Ultramicrosc. 96 (2003) 335.
[9] M. Saito, K. Kimoto et al., J. Electron Microsc. in print (2009)
[10] K. Kimoto et al., Appl. Phys. Lett. 94 (2009) 041908.
[11] This research is partly supported by JST-CREST and Nano-net by MEXT.

Basic Questions involved in Electron-Induced Sputtering

R.F. Egerton[1,2], R. McLeod[1,2], F. Wang[2], and M. Malac[1,2]

[1] Department of Physics, University of Alberta, Edmonton, Canada T6G 2G7.
[2] National Institute for Nanotechnology, Edmonton, Alberta, Canada T6G 2M9.

Radiation damage is the main factor determining the ultimate spatial resolution of any microscopy or spectroscopy that uses electron beams. Damage is by radiolysis in insulating materials but by knock-on displacement in conducting solids.

Displacement of surface atoms (electron-induced sputtering) occurs for incident energies above a threshold E_0^{min} that depends on the atomic weight and displacement energy E_d of surface atoms; it lies below 300 keV for the majority of elements and is therefore of concern when electrons are focused into a sub-nm TEM probe and incident onto semiconducting or metallic specimens.

E_d is often taken as the sublimation energy E_{sub} per atom but this assumption is questionable since sublimation removes atoms at kink sites of lower binding energy; for sputtering from a flat surface, a better approximation may be $E_d \sim (5/3)E_{sub}$.

Taking $E_{sub} = 3.8$ eV for gold, the surface binding energy is then $E_d \sim 6.3$ eV and $E_0^{min} = 407$ keV, comparable to the 350keV experimental estimate [1]. We have confirmed the absence of sputtering at 300 keV, which would be above the threshold (270 keV) if E_d were equal to E_{sub}.

Taking $E_d = (5/3)(2.95\text{eV})$ for silver gives $E_0^{min} = 202$ keV. Braidy et al. [2] observed e-beam sputtering of silver particles (6nm to 14nm diameter) at 200 keV but curved surfaces have a greater fraction of atoms at step sites, approximately $f \approx 2(h/R)^{1/2}$ for atoms of diameter h on a spherical particle of radius R. On this basis, we can expect E_d and E_0^{min} to be substantially lower for particles of diameter below 10nm.

Another uncertainty concerns the geometry of the escape potential $E_d(\phi)$, where ϕ is the angle between the momentum transfer and the surface-normal. A spherical potential corresponds to E_d independent of ϕ whereas E_d is proportional to $1/\cos^2\phi$ for a planar surface potential. In the latter case, E_0^{min} increases for non-normal electron incidence, so sputtering should be slower at the edges of a particle, leading to a flattened particle shape.

Even for perpendicular incidence, the form of $E_d(\phi)$ affects the sputtering rate by a factor of about three [3]. The angular dependence of $E_d(\phi)$ can be estimated from molecular-dynamics calculations, which in the case of a carbon nanotube [4] suggest an escape potential that is intermediate between the planar and spherical cases.

References

[1] D. Cherns, Surface Science 90 (1979) 339.
[2] N. Braidy et al., Microsc. Microanal. 14, 166 (2008).
[3] R.F. Egerton et al., Microsc. Microanal. 12, 65-71 (2006).
[4] A. Zobelli et al., Phys. Rev. B75, 245402 (2007).

Energy Loss Characterisation of Nanostructures in 2D and 3D

W. Guan, M. A. Mat Yajid, T. Gnanavel, Z. Saghi, Y. Peng, X. Xu, G. Möbus

Department of Engineering Materials, University of Sheffield, Mappin Street, Sheffield S1 3JD, UK

The availability of high tilt specimen holders has enabled the full 3D viewing of specimens which are shaped to be electron transparent in all viewing directions. The obvious application is for tomography, but not limited to it, and the two techniques of 3D viewing and EELS chemical analysis can be mutually beneficial in many ways.

In a first application, we apply EFTEM low loss imaging in 3D for the reconstruction of C-Al core shell nanoobjects including single and double excitation plasmon resonances, carbon resonance and a surface-plasmon related signal. Options for combining more than one energy loss levels to generate advanced tomograms are discussed.

In another application we present EELS analysis of hole drilling events in thin metal films, viewed in perpendicular direction to image material re-deposition outside the original specimen volume, as a result of which we can exclude carbon growth as origin of growth of surface pillars.

Finally FIB-shaping of metallic multilayers into 3D nanopillars, consisting of arrays of 0D metallic dots, is examined using EELS line scans in low loss mode. The aim of the research is to study the influence of dimensionality on alloy formation reactions. The samples are therefore analysed before and after in-situ and ex-situ heat treatments at various temperatures. Cu-Al and Cu-Al-Ti metallurgy is explored and reaction products compared to traditional bulk metallurgy.

In conclusion, 3D chemical nano-analysis techniques based on EELS, which have been introduced almost 10 years ago, can be designed in two ways:

(i) choose a 3D imaging technique and turn it chemically sensitive by linking to EELS.
(ii) choose a 2D EELS based imaging mode and turn it into a 3D signal.

A “matrix” of techniques and modes will be developed helping in classification and derivation of future trends.